JOURNAL OF PETROLOGY | VOLUME 49 | NUMBER 4 | PAGES 615–632 | 2008 | doi:10.1093/petrology/egm052

Origin of the Oceanic Lithosphere

DEAN C. PRESNALL[1,2,3]* AND GUDMUNDUR H. GUDFINNSSON[2,3]

[1]DEPARTMENT OF GEOSCIENCES, UNIVERSITY OF TEXAS AT DALLAS, PO BOX 830688, RICHARDSON, TX 75083-1305, USA

[2]GEOPHYSICAL LABORATORY, 5251 BROAD BRANCH ROAD, NW, WASHINGTON, DC 20015, USA

[3]BAYERISCHES GEOINSTITUT, UNIVERSITÄT BAYREUTH, D-95440 BAYREUTH, GERMANY

RECEIVED DECEMBER 6, 2006; ACCEPTED AUGUST 8, 2007
ADVANCE ACCESS PUBLICATION NOVEMBER 22, 2007

In a global examination of mid-ocean ridge basalt (MORB) glass compositions, we find that Na_8–Fe_8–depth variations do not support modeling of MORBs as aggregates of melt compositions generated over a large range of temperature and pressure. However, the Na_8–Fe_8 variations are consistent with the compositional systematics of solidus melts in the plagioclase–spinel lherzolite transition in the CaO–MgO–Al_2O_3–SiO_2–Na_2O–FeO (CMASNF) system. For natural compositions, the P–T *range for melt extraction is estimated to be ~1·2–1·5 GPa and ~1250–1280°C. This* P–T *range is a close match with the maximum* P–T *conditions for explosive pressure-release vaporization of carbonate-bearing melts. It is proposed that fracturing of the lithosphere induces explosive formation and escape of CO_2 vapor. This provides the vehicle for extraction of MORBs at a relatively uniform* T *and* P. *The upper portion of the CO_2-bearing and slightly melted seismic low-velocity zone flows toward the ridge, rises at the ridge axis to lower-lithosphere depths, melts much more extensively during this rise, and releases MORB melts to the surface driven by explosively escaping CO_2 vapor. The residue and overlying crust produced by this melting then migrate away from the ridge axis as new oceanic lithosphere. The entire process of oceanic lithosphere creation involves only the upper ~140 km. When lithospheric stresses shift fracture formation to other localities, escape of CO_2 ceases, the vehicle for transporting melt to the surface disappears, and ridges die. Inverse correlations of Na_8 vs Fe_8 for MORB glasses are explained by mantle heterogeneity, and positive variations superimposed on the inverse variations are consistent with progressive extraction of melts from short, ascending melting columns. The uniformly low temperatures of MORB extraction are not consistent with the existence of hot plumes on or close to ocean ridges. In this modeling, the southern Atlantic mantle from Bouvet to about 26°N is relatively homogeneous, whereas the Atlantic mantle north of about 26°N shows significant long-range heterogeneity. The mantle between the Charlie Gibbs and Jan Mayen fracture zones is strongly enriched in FeO/MgO, perhaps by a trapped fragment of basaltic crust. Iceland is explained as the product of this enrichment, not a hot plume. The East Pacific Rise, Galapagos Ridge, Gorda Ridge, and Juan de Fuca Ridge sample mantle that is heterogeneous over short distances. The mantle beneath the Red Sea is enriched in FeO/MgO relative to the mantle beneath the northern Indian Ocean.*

INTRODUCTION

A major development in the characterization of mid-ocean ridge basalt (MORB) glass compositions was the discovery that Na_8 and Fe_8 (Na_2O and FeO normalized to a constant MgO value of 8%) show systematic variations when plotted against each other and against axial ridge depth (Klein & Langmuir, 1987, 1989; Langmuir *et al.*, 1992). The model developed in these papers to explain the Na_8-Fe_8-depth systematics involves melting columns that start at varying depths, require large variations in potential temperature, and extend to low pressures near the base of the crust. According to this modeling, longer columns produce more melt, a thicker crust (considered to be indicated by shallower axial ridge depths), lower Na_8, higher Fe_8, and higher potential temperatures. These correlations, called the global systematics, were attributed to melting columns with a wide range of initial pressures ranging from about 1·2 to 4 GPa and a potential temperature variation of ~1260 – 1590°C. For their global plots of chemistry vs axial ridge depth, each data point was an average of chemistry and depth over ~100 km of ridge length, and the trends were considered to be applicable to ridge lengths of hundreds to thousands of kilometers (Langmuir *et al.*, 1992, p. 204). Also, 'local' trends, applicable to ridge lengths less than ~100 km, were reported that have positive

*Corresponding author. Present address: Department of Geosciences, University of Texas at Dallas, PO Box 830688, Richardson, TX 75083-1305, USA. E-mail: presnall@utdallas.edu

correlations of Na_8 vs Fe_8 cutting across the inverse global trends of Na_8 vs Fe_8. For plots of local trends, Na_8 and Fe_8 values were calculated for single analyses. Langmuir *et al.* (1992, p. 249) were unable to find a satisfactory explanation for the local trends.

Klein & Langmuir (1987) and Langmuir *et al.* (1992) noted that the Azores region on the Mid-Atlantic Ridge, considered by some to be a major plume, does not conform to their 'normal' systematics. Also, the Galapagos Ridge passes close to the Galapagos Islands, another plume candidate. This ridge shows an increase of Na_8 and decrease of Fe_8 with decreasing axial depth (Langmuir *et al.*, 1992; Detrick *et al.*, 2002), the opposite of the trend predicted by the Klein & Langmuir (1987, 1989) and Langmuir *et al.* (1992) modeling. Because of these issues, the global correlations were applied only to ridges 'not . . . substantially influenced by hot spots' (Langmuir *et al.*, 1992, p. 200). Despite this, Iceland, commonly considered to be the strongest plume candidate anywhere along the oceanic ridge system, was noted as being consistent with the global systematics (Langmuir *et al.*, 1992, fig. 15 caption). In view of the growing controversy over the existence of mantle plumes (e.g. Foulger *et al.*, 2005*b*), the Na_8–Fe_8–depth systematics are re-examined here at all scales from global to local. To develop a general model that explains the chemistry of basalts along all ridge segments, samples considered by some to be at or close to plumes are not excluded. The solidus phase relations of model lherzolite in the system CaO–MgO–Al_2O_3–SiO_2–Na_2O–FeO (CMASNF) are integrated with the strong effect of CO_2 on solidus relationships to extend the model of Presnall *et al.* (2002) for the generation of MORBs. We then combine this chemical modeling with the physical context of mid-ocean ridge development that begins with initial fracture formation in the oceanic lithosphere, evolves to full maturity of an active ridge, and ends with decline and termination in favor of other new ridges.

DATA

The global database of MORB glass analyses assembled by the Smithsonian Institution, http://www.minerals.si.edu/research/glass/vgdf.htm (Magma Batch File, version 100199), provides an opportunity to examine the Na_8–Fe_8–depth systematics using data from a single microprobe facility free of inter-laboratory analytical differences. By using only this source of data, more comprehensive coverage is sacrificed, but a high level of internal consistency is gained. The data were filtered to delete samples with no age or depth information and samples from seamounts, trenches, and back-arc basins. Data from seamounts were excluded because many of the plots show composition vs sampling depth, which is used as an approximation of axial ridge depth. Samples from seamounts would skew the results for these plots toward incorrectly shallow ridge depths. Analyses of samples $\leq$1 Ma in age were retained. This left a database overwhelmingly dominated by tholeiitic compositions but with 11 alkalic samples, four from the Atlantic Ocean, one from the Indian Ocean, and six from the Pacific Ocean. We followed the Klein & Langmuir (1987, 1989) and Langmuir *et al.* (1992) procedure of retaining only analyses with MgO between 5% and 8·5%. This eliminated two alkalic samples from the Pacific, leaving four from the Atlantic Ocean, four from the Pacific Ocean, and one from the Indian Ocean. Of the two that were eliminated on the basis of MgO content, one has a total lower than 98·5%. All the others have totals between 98·5 and 101·5%. This means that subsequent filtering on the basis of totals $<$98·5 to $>$101·5% had no effect on the number of alkalic samples, because the only one with a low total also has MgO $<$5%. Deletion of samples with totals $<$98·5% removed 21 samples: nine from the Atlantic Ocean, four from the Indian Ocean, six from the Pacific Ocean, and three from the Caribbean Sea. These samples may have contained high amounts of H_2O, but their omission would not significantly alter the trends we show because of the small number of samples and their fairly even distribution over the oceans. The final dataset has 1700 samples. Following the procedure of Langmuir *et al.* (1992, pp. 199–200 and fig. 14 caption), the Fe_8 and Na_8 values have been adjusted upward by 5% and 7·5% of the amount present, respectively. Use of these adjustments does not imply that the Smithsonian data are considered to be in error. Our intent is merely to allow direct comparison of the plots presented here with those of Langmuir *et al.* (1992). Values for Na_8 and Fe_8 have been calculated for each analysis using the equations of Klein & Langmuir (1987, p. 8092).

Instead of plotting axial ridge depth and MORB glass chemistry averaged over about 100 km of ridge length, as done by Klein & Langmuir (1987, 1989) and Langmuir *et al.* (1992) for their global plots, the procedure of Brodholt & Batiza (1989) and Niu & Batiza (1991), who plotted sampling depth and chemical data for single samples or averages of several samples considered to be taken from the same lava flow, has been followed. Although plots of unaveraged data produce enhanced scatter, Brodholt & Batiza (1989) found that such plots show the same Na_8–Fe_8 systematics as the plots of Klein & Langmuir (1987) based on averaged data. Klein & Langmuir (1989, pp. 4241–4242) pointed out that such plots are dominated by more thoroughly sampled ridges and are therefore biased. However, plots of averaged data also have a statistical problem because each point is an average of a different number of samples and therefore has a different statistical weight. We prefer plots of unaveraged data because they give a better visual understanding of the density and distribution of the data, especially on plots of Na_8 and Fe_8 vs distance along a ridge. Linear least-squares

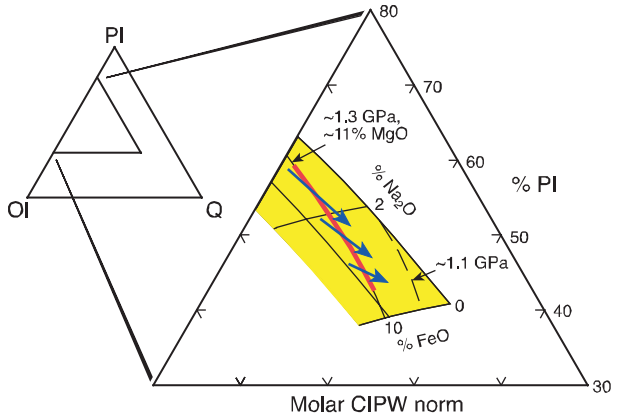

Fig. 1. Molar CIPW normative projection of the solidus surface (ol + opx + cpx + pl + sp + liq) of model lherzolite in the system $CaO–MgO–Al_2O_3–SiO_2–Na_2O–FeO$ (CMASNF) onto the plagioclase (Pl) – olivine (Ol) – quartz (Q) base of the tholeiitic basalt tetrahedron Pl–Ol–Di–Q at 0·93–1·5 GPa, modified after Presnall *et al.* (2002). The algorithm for plotting points in this diagram is given in Presnall *et al.*, (2002, Fig. caption 6). Data for the FeO-free boundary are from Walter and Presnall (1994). Data for the Na_2O–free boundary are from Gudfinnsson and Presnall (2000). Approximate contours of 2% Na_2O and 10% FeO are drawn parallel to the Na_2O–free and FeO–free boundaries, respectively. The corner of the surface labeled 0 (for 0% FeO and 0% Na_2O) is the 0·93 GPa invariant point liquid for the assemblage ol + opx + cpx + pl + sp + liq in the system, $CaO–MgO–Al_2O_3–SiO_2$ (Presnall *et al.*, 1979; Walter and Presnall, 1994). This marks the transition along the 4-component solidus between plagioclase lherzolite and spinel lherzolite. The two lines extending from this point show the composition ranges of liquids along the 5-space plagioclase-spinel lherzolite transition interval for the systems $CaO–MgO–Al_2O_3–SiO_2–FeO$ and $CaO–MgO–Al_2O_3–SiO_2–Na_2O$. This shows how solidus liquid compositions for the plagioclase-spinel lherzolite transition, when projected into CIPW molar normative space, change from a point in 4-space to a line in 5-space, and finally to a surface in 6-space. The 1·3 GPa and 11% MgO contours are nearly identical and are shown as a single line. The red curve shows an inverse correlation of Na_2O and FeO (the 'global' trend), and is drawn on top of the 11% MgO contour. Blue lines show positive correlations of Na_2O and FeO (the 'local' trend), which all converge at the 0% FeO, 0% Na_2O corner of the yellow solidus surface.

lines are fitted to many of the plots, but because the data are widely scattered, the equations for these lines are not given. Our analysis is limited to a rough determination of whether a trend is positive, inverse, or neutral.

PHASE RELATIONS

In Fig. 1, the yellow region shows approximate six-space compositions of solidus melts in equilibrium with olivine, enstatite, diopside, spinel, and plagioclase (the plagioclase–spinel lherzolite transition) as they appear when projected into the CIPW molar normative tetrahedron, Ol–Di–En–Q, and then onto the Ol–Di–Q base of this tetrahedron. The algorithm used for this projection is given in Presnall *et al.* (2002, fig. 6 caption). In this diagram, contours of pressure are nearly parallel to contours of constant MgO of the solidus melt. Approximate contours of 1·1 and 1·3 GPa are indicated, and the contour of 11% MgO on the solidus is almost coincident with the 1·3 GPa contour. For purposes of this discussion, the two contours are shown as a single line. When melts are generated at constant pressure, the amount of MgO for the extracted melt is nearly constant and Na_2O is inversely correlated with FeO. Also, at constant pressure, CaO/Al_2O_3 decreases with increasing Na_2O and decreasing FeO (not shown in Fig. 1, but see Presnall *et al.*, 2002, fig. 13). Thus, as noted by Presnall *et al.* (2002), the 'global' systematics of Na_2O, FeO, and CaO/Al_2O_3 at an MgO value of 8% have the same form as the systematics of solidus melts generated at constant pressure in the plagioclase–spinel lherzolite transition of the CMASNF system.

Langmuir *et al.* (1992, p. 243) concluded, on the basis of a generalized argument, that the Na_8–Fe_8 inverse correlation cannot be produced by mantle heterogeneity. However, the phase relations in the CMASNF system (Fig. 1) show that if initial melts are generated in the plagioclase–spinel lherzolite transition region at an approximately constant pressure, an inverse correlation of Na_2O vs FeO does not merely permit heterogeneity of the source composition, it is required. However, these phase relations were not available in 1992. Because natural compositions deviate very little from this system, we believe this is also a very strong constraint for melting processes at mid-ocean ridges.

The short blue lines on the solidus that cut across the red line in Fig. 1 are schematic curves that trace the changing compositions of melts produced during polybaric fractional melting of different source compositions. These curves, if extended, would all converge at 0% FeO and 0% Na_2O, which is the invariant point marking the plagioclase–spinel lherzolite transition in the CMAS system. They describe the polybaric composition paths of melts extracted from source regions that become progressively more depleted as pressure decreases a small amount along short melting columns. For each column, a series of melts would be produced with a positive variation of Na_8 with Fe_8 [the 'local' Na_8 vs Fe_8 correlation of Klein & Langmuir (1989) and Langmuir *et al.* (1992)]. Each path would produce a different range of Fe_8 and Na_8 values depending on the initial composition of the source. Progressive melt extraction from a rising melting column would steadily increase its MgO/FeO ratio, so that the melts highest in MgO/FeO would be expected from the shallowest part of the column. This result is the opposite of the assumption sometimes made that melts high in MgO/FeO are an indication of melting at great depths. For a heterogeneous mantle, an increase in the MgO/FeO ratio of melts would also occur along the red line as the normative proportion of quartz decreases. Thus, magnesian olivine could also crystallize from an early melt low in normative quartz.

These phase relations show that positive correlations of Na_8 with Fe_8 are produced by melt extraction over

a small pressure range from rising melting columns, whereas inverse correlations are produced by melt extraction at roughly constant pressure from a heterogeneous mantle. Because MgO of the liquid remains essentially constant along an isobar on the solidus as FeO of the liquid increases, melts that have progressively higher Fe_8 are produced from increasingly fertile sources that are progressively higher in FeO/MgO. The low Na_8 values of these melts are imposed by the phase relations. Note also that only the form of the systematics on the solidus is the same as the systematics observed in MORB glasses, not the absolute values of Na_2O, FeO, and MgO. This is consistent with the design of the normalization procedure invented by Klein & Langmuir (1987). By locating their normalization at an intermediate stage of fractional crystallization, they intended to reveal only a projected image of the compositional systematics at the source. Thus, the values of FeO and Na_2O at MgO = 8% will be higher than the values of FeO and Na_2O produced at the source. For the same reason, the MgO value at the source will be higher than 8%. These differences are consistent with the values shown in Fig. 1. The remarkable consistency of the systematics shown by the phase relations at the solidus (Fig. 1) with the systematics observed in MORB glasses strongly supports the validity of their normalization procedure as a scheme that screens out the compositional variations caused by low-pressure fractional crystallization and reveals the systematics of melting at the source.

The phase relations shown in Fig. 1 have some uncertainties. The contours of melt composition across the surface are, at present, constrained only by the bounding lines for the systems CaO–MgO–Al_2O_3–SiO_2–Na_2O (Walter & Presnall, 1994) and CaO–MgO–Al_2O_3–SiO_2–FeO (Gudfinnsson & Presnall, 2000). As these lines in the normative plot have little curvature, the surface they bound is also expected to have little curvature. The contours of FeO and Na_2O across the surface are approximate, but their general form must be as shown. Addition of Cr_2O_3 to the system would extend the stability field of ol + opx + cpx + plag + sp + liq to 1 atm (Libourel, 1991), a change expected to apply also to fully complex natural peridotite compositions. The effects of TiO_2, P_2O_5, and K_2O are unknown. Despite these various issues, the CMASNF system contains all of the major phases in the source (olivine, enstatite, diopside, plagioclase, spinel), and about 99% of the composition of both basalts and lherzolites. Therefore, the phase relations in this system, when considered from the viewpoint of either the bulk composition or the mineralogy, are a robust constraint on the melting behavior of the mantle in this pressure range.

The most important sources of major-element heterogeneity in the upper mantle are probably subducted basaltic crust and depleted mantle material that lies directly beneath this crust. For model basaltic compositions in the CMAS basalt tetrahedron, Liu & Presnall (2000) found that garnet first appears at the solidus of basaltic compositions at a pressure of about 1·8–1·9 GPa. In results consistent with this, Pertermann & Hirschmann (2003*a*, 2003*b*) found garnet in equilibrium with melt for a basaltic composition at 2 GPa. Therefore, at $P < \sim 1{\cdot}8$ GPa, a region of basaltic bulk composition in this pressure range would have the same mineral assemblage as lherzolite, ol + opx + cpx + sp + plag, but the proportions and compositions of these minerals would be different. Therefore, at pressures of about 0·9–1·5 GPa in six-space, the solidus surface shown in Fig. 1 would govern the melting relations of a mantle with the bulk composition of a basalt, a depleted lherzolite, an enriched lherzolite, any mixture of these, and even any positive proportion of the five crystalline phases. An important aspect of the phase equilibrium controls in the pressure range of the plagioclase–spinel lherzolite transition is that basaltic melts of closely similar bulk composition would be produced even though significant mantle heterogeneity may exist. These controls would prevail as long as all five crystalline phases are present in the source. The geometrical relationships that lead to this conclusion have been discussed by Presnall (1969). Thus, for a fragment of basalt subducted into the mantle and partially melted along with some adjacent lherzolite and/or harzburgite at pressures less than ~1·5 GPa, the melt produced would be basaltic and would differ in only minor ways from the composition of a typical MORB. Depending on the amount of thermal energy available and the proportion of lherzolite to basalt in the source, the amount of melt erupted could be a very large proportion of the source. This feature of the melting behavior will be discussed below in relation to the production of basalts at Iceland.

NA_8–FE_8–DEPTH VARIATIONS

Atlantic ridge system

Variations of Na_8 with Fe_8 for the entire Atlantic ridge system are shown in Fig. 2. These appear as a set of rough positive Na_8–Fe_8 trends that are stacked along an overall inverse Na_8–Fe_8 trend. This is consistent with the plots of Klein & Langmuir (1989) and Langmuir *et al.* (1992). To examine the Atlantic ridge system in more detail, we have broken it into segments of varying lengths based on the locations of tectonic features along the ridge system. From south to north, these segments are: (1) the southern part of the Mid-Atlantic Ridge, extending from the Bouvet triple junction at about 55°S to the southern limit of the Azores swell at about 26°N; (2) the Azores region of the North Atlantic; (3) the Reykjanes Ridge just south of Iceland, the Kolbeinsey Ridge just north of Iceland, and a few submarine samples from the Iceland platform; (4) the Mohns Ridge. The Azores region is separated from the Reykjanes Ridge by the large offset of the Charlie Gibbs

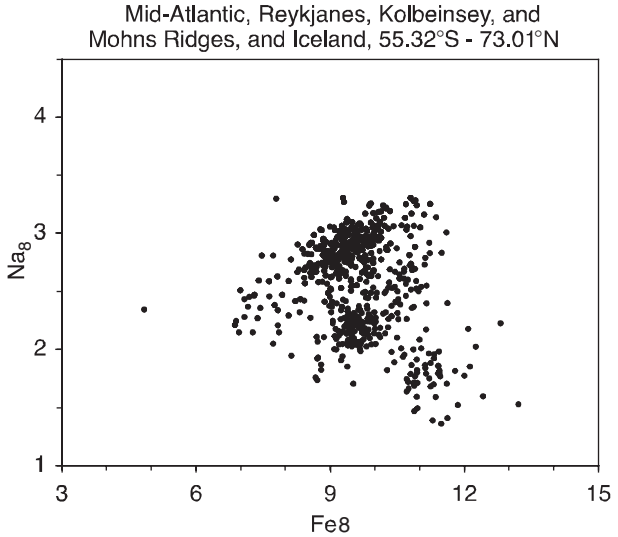

Fig. 2. Na_8 versus Fe_8 for the Atlantic ridge system from the Bouvet triple junction to the Mohns Ridge.

Fracture Zone. The Kolbeinsey Ridge is separated at its northern limit from the Mohns Ridge by the Jan Mayen Fracture Zone, which also has a large offset.

For the 9100 km segment of the southern Mid-Atlantic Ridge from Bouvet to 27°N, the correlation of Na_8 with Fe_8 is positive (Fig. 3a) and the overall trend lies near the high Na_8 and low Fe_8 end of the inverse Atlantic array. The Azores region also shows a correlation that is generally positive but somewhat diffuse (Fig. 3b), in this case for a ridge segment of about 2800 km; and the overall trend is offset to lower Na_8 and slightly higher Fe_8 values. Most of the Azores data appear to be lower in Na_8 and higher in Fe_8 than data from the South Atlantic. Data from the 2000 km Reykjanes–Iceland–Kolbeinsey ridge segment (Fig. 3c) show no correlation at all between Na_8 and Fe_8, and the overall average for this region is significantly lower in Na_8 and higher in Fe_8. The most northerly ridge segment, the Mohns Ridge just north of the Jan Mayen Fracture Zone, shows a reversal back to higher Na_8 and lower Fe_8 values (Fig. 3d), but the data are too sparse to determine if any trend between Na_8 and Fe_8 exists.

Figure 3e shows variations of Na_8 vs Fe_8 for three short ridge segments, all less than 60 km long. One lies south of the Azores swell at about 24°N, one is just south of the Azores, and a third is just off the southern shore of Iceland on the submarine portion of the Iceland platform. Figure 3a–e shows that a positive Na_8–Fe_8 correlation can be very distinct for ridge segments less than 60 km. As the ridge segments increase in length, the offset positive correlations merge into an overall inverse Na_8–Fe_8 correlation for the entire ridge (Fig. 2) that is made more diffuse by the positive local trends. This continuous gradation between local and global trends reconciles the original description of these trends as 'local' (Klein & Langmuir, 1989) with the result of Niu & Batiza (1993) that positive Na_8–Fe_8 trends can occur for ridge lengths that are both local and global.

South of the Charlie Gibbs Fracture Zone, we have not found any inverse Na_8–Fe_8 correlations for short ridge segments. An inverse correlation becomes evident only when data for the entire Atlantic ridge system are plotted together. We interpret these systematics to indicate that major-element mantle heterogeneity is minimal over small ridge lengths and becomes more evident as ridge lengths increase. The positive Na_8–Fe_8 trends are modeled as the result of short diapirs that become progressively more depleted as they ascend and produce melts with positive Na_8–Fe_8 correlations and progressively lower Na_2O and FeO (blue arrows in Fig. 1). The progressive depletion of such diapirs would decrease their density (Presnall & Helsley, 1982) relative to older and cooler mantle on the flanks of the ridge, which would induce further ascent and melting.

Figure 3c shows that basalts from the region between the Charlie Gibbs and Jan Mayen fracture zones have combined Na_8 and Fe_8 values that produce a clean separation from almost all other basalts in the Atlantic. On the basis of the phase relations in Fig. 1, this indicates a source that is strongly enriched in FeO and unusually low in MgO/FeO. This is consistent with the proposal of Foulger *et al.* (2005*a*) that basaltic crust was trapped in the Caledonian suture beneath the ridge in this region and became part of the source for the enhanced melt productivity at Iceland. Melts from such a source would be strongly enriched in Fe_8 and phase relations at the solidus (Fig. 1) would impose the production of melts depleted in Na_8. In the pressure range of the plagioclase–spinel lherzolite transition, the mineralogy of a combined lherzolite–basalt source would be the same as that of a lherzolite, but with different proportions and compositions of the phases. Thus, basalt compositions broadly similar to normal MORB compositions would be produced, but the volume of these melts at comparable temperatures of melt extraction would be significantly increased (Presnall, 1969). Seismic data (Ritsema & Allen, 2003) consistent with this interpretation show an anomalous upper mantle that extends both north and south well beyond the Icelandic platform.

For the same sequence of ridge segments from south to north discussed above, Fig. 4 shows the variations of Na_8 and Fe_8 with sampling depth. The southern Atlantic extending to 26°N shows no correlation of either Na_8 or Fe_8 with depth (Fig. 4a). For the Azores region, Na_8 and Fe_8 both increase with depth (Fig. 4b). These trends are contrary to the modeling of Klein & Langmuir (1987, 1989) and Langmuir *et al.* (1992). For the Reykjanes–Iceland–Kolbeinsey segment, Na_8 increases slightly and

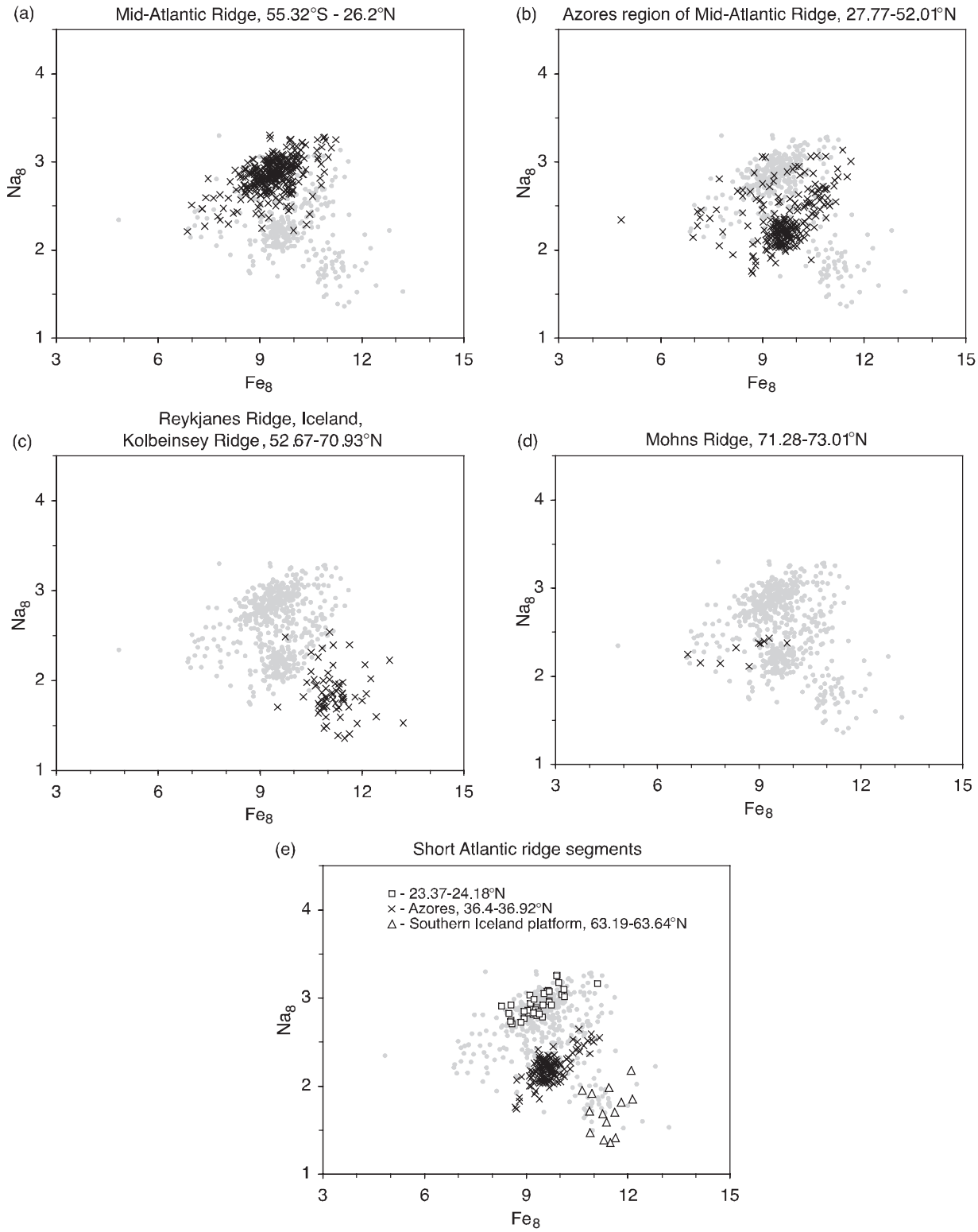

Fig. 3. Na_8 versus Fe_8 for different segments of Atlantic ridges against a background of the total remaining Atlantic ridge samples from the Bouvet triple junction to the Mohns Ridge (gray circles).

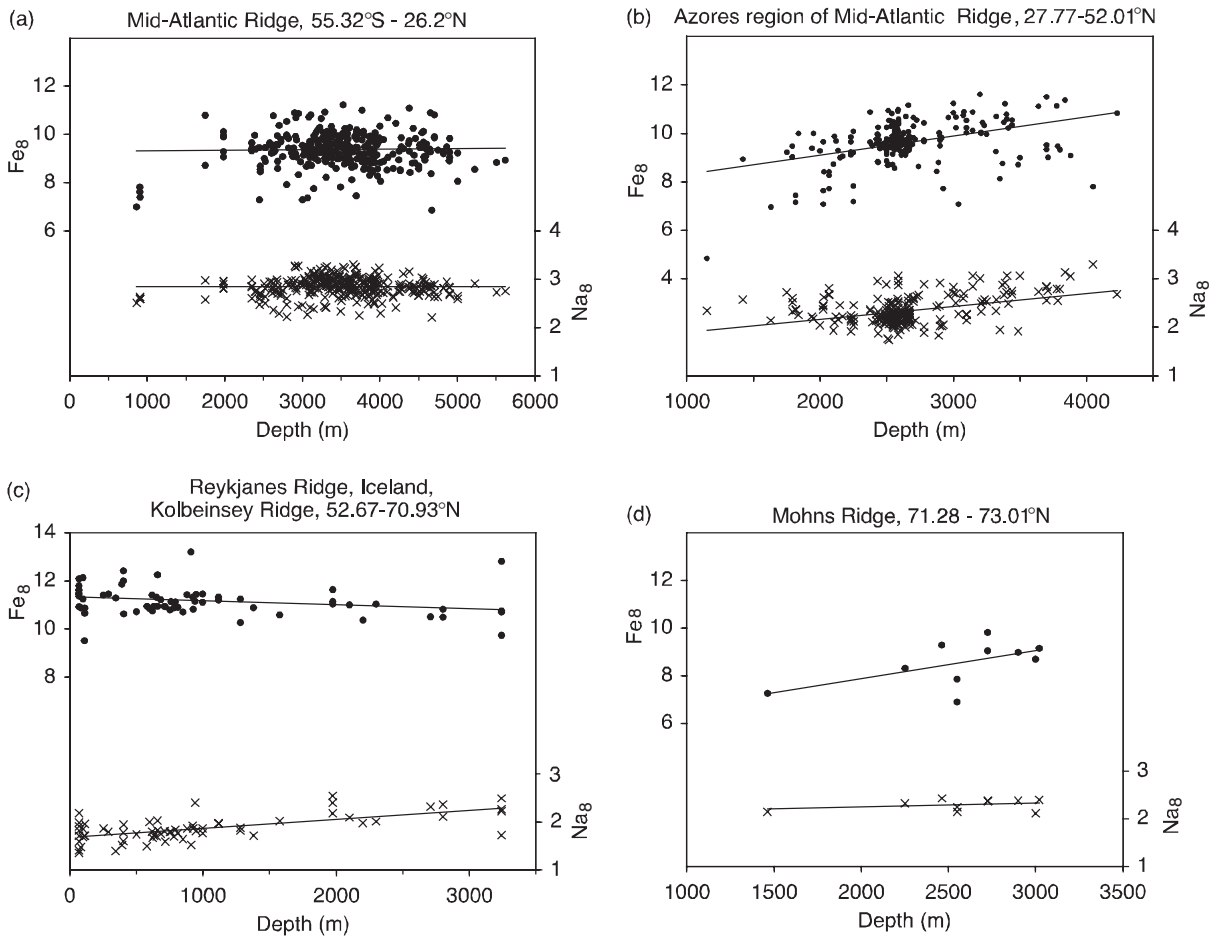

Fig. 4. Na_8 and Fe_8 versus sampling depth for different segments of Atlantic ridges (crosses, Na_8; circles, Fe_8).

Fe_8 shows essentially no variation (Fig. 4c), again in disagreement with the systematics of Klein & Langmuir (1987, 1989) and Langmuir *et al.* (1992). Data for the Mohns Ridge are more sparse and uncertain (Fig. 4d). However, data south of the Charlie Gibbs Fracture Zone (Fig. 4a and b) are sufficiently abundant to show that the entire 11 900 km Mid-Atlantic Ridge is anomalous in the Klein & Langmuir (1987, 1989) and Langmuir *et al.* (1992) model, not just the Azores.

Na_8 and Fe_8 values for the Atlantic ridge system as a function of latitude (Fig. 5) illustrate the features already discussed from a slightly different perspective. For the two ridge segments of 'global' length scale, the Azores region and the Mid-Atlantic Ridge south of the Azores, the increases and decreases of Na_8 and Fe_8 with latitude are roughly parallel. This parallel tracking of Na_8 and Fe_8 with latitude mirrors the parallel tracking with sampling depth (Fig. 4a and b). Although the Mid-Atlantic Ridge south of 27°N has large sampling gaps, the Fe_8 data in Fig. 5 suggest that the mantle changes little in MgO/FeO. Between 27°N and the Charlie Gibbs Fracture Zone, the MgO/FeO ratio increases as the Azores are approached from both the north and south (Fig. 5), a result consistent with the observation of Dick *et al.* (1984) that abyssal peridotites along the ridge close to the Azores at 43°N are more depleted than those farther away at 23°N.

At the Charlie Gibbs Fracture Zone, Fe_8 and Na_8 both change abruptly and in opposite directions. Then, at the Jan Mayen Fracture Zone, these change are reversed (Fig. 5). The direction of both of these changes is consistent with the Klein & Langmuir (1987, 1989) and Langmuir *et al.* (1992) global systematics but represents an abrupt and unexplained departure from the inability of their modeling to explain the entire 11 900 km Mid-Atlantic ridge south of the Charlie Gibbs Fracture Zone. However, it is a straightforward continuation of our modeling to attribute the abrupt inverse changes in Na_8 and Fe_8 at these transforms to mantle heterogeneity simultaneously with production of positive Na_8–Fe_8 correlations to the south by extraction of melts from short melting columns (Fig. 1).

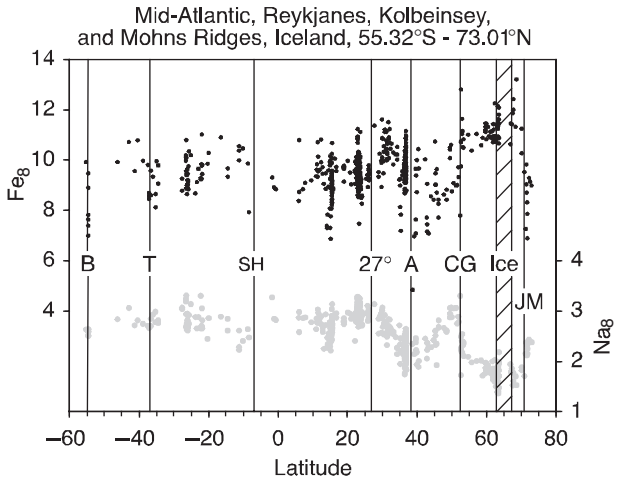

Fig. 5. Na_8 and Fe_8 versus latitude for Atlantic ridges. B, Bouvet; T, Tristan da Cunha; SH, St. Helena; A, Azores; CG, Charlie Gibbs Fracture Zone; Ice, Iceland platform to 500 m contour below sea level; JM, Jan Mayen Fracture Zone.

A similar discontinuity of Na_8 and Fe_8 across a transform fault with a large offset on the Southwest Indian Ridge has also been attributed to an abrupt change in the mantle composition (Mayzen *et al.*, 2003).

South American–Antarctic and Southwest Indian Ridges

In combination with the southern Mid-Atlantic Ridge, basalt glasses from the South American–Antarctic and Southwest Indian Ridges sample the mantle on three sides of the Bouvet triple junction. The compositions overlap the high Na_8 and low Fe_8 extreme of the Atlantic array and extend it slightly to even higher Na_8 values (Fig. 6a). As was found for the southern part of the Atlantic Ridge, Fe_8 and Na_8 track parallel to each other when plotted against depth (Fig. 6b), which continues the lack of support for the Klein & Langmuir (1987, 1989) and Langmuir *et al.* (1992) modeling along the Atlantic ridge system. For these combined ridges, there is a small decrease of Na_8 eastward, but no change in Fe_8 (Fig. 6a and c).

East Pacific Rise

An inverse correlation of Na_8 vs Fe_8 occurs for the East Pacific Rise as a whole (Fig. 7a), but the slight decrease of Na_8 and slight increase of Fe_8 with depth (Fig. 7b) are the opposite of the Klein & Langmuir (1987, 1989) and Langmuir *et al.* (1992) modeling. Although the depth trends are weak and dominated by data in the narrow range of about 2500–3000 m, they are supported by other Pacific data at depths of 3500–5600 m (Batiza *et al.*, 1995). These trends continue the result for the Atlantic ridges in showing no support for the Klein & Langmuir (1987, 1989) and Langmuir *et al.* (1992) modeling. No systematic variations of either Na_8 or Fe_8 with latitude are evident (Fig. 7c).

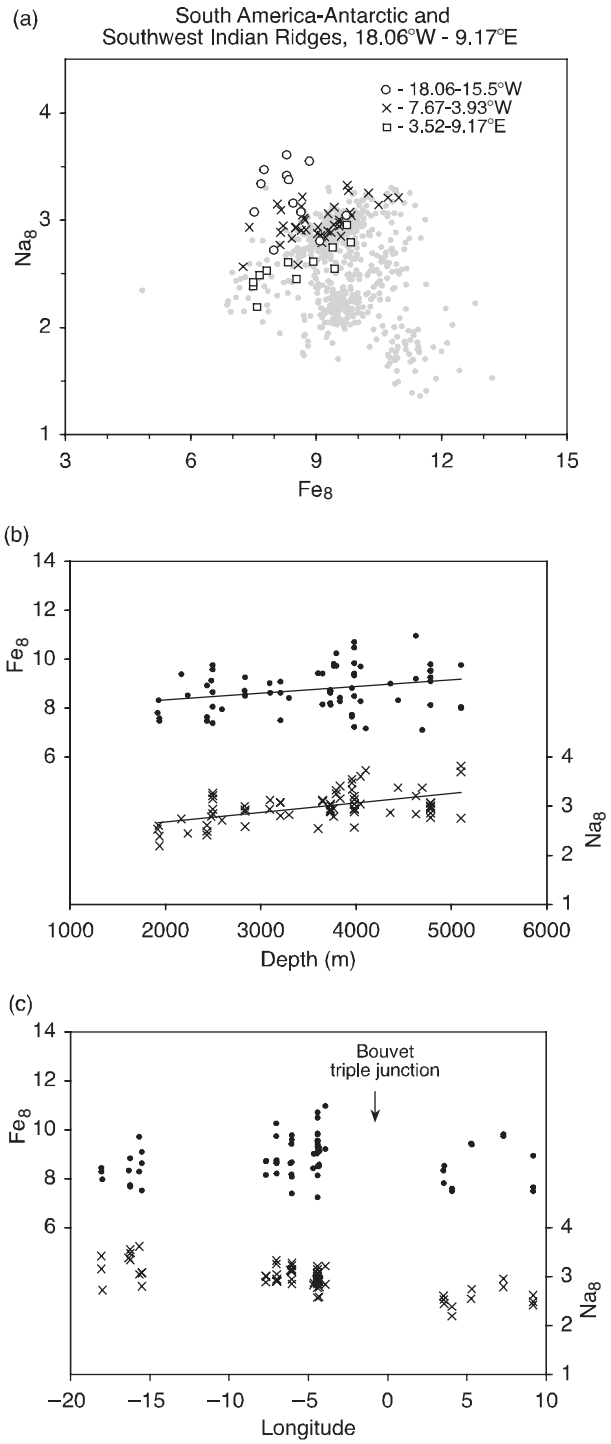

Fig. 6. South American-Antarctic and Southwest Indian Ridges. (a) Na_8 versus Fe_8. Gray circles are data for all Atlantic ridges. (b) Na_8 and Fe_8 versus sampling depth. (c) Na_8 and Fe_8 versus longitude.

Two small and adjacent areas where data are especially dense provide an interesting contrast. For the ridge segment from 10·74 to 11·64°N, the plot of Na_8 vs Fe_8 forms a small cluster with no trend (Fig. 7d), and there is no

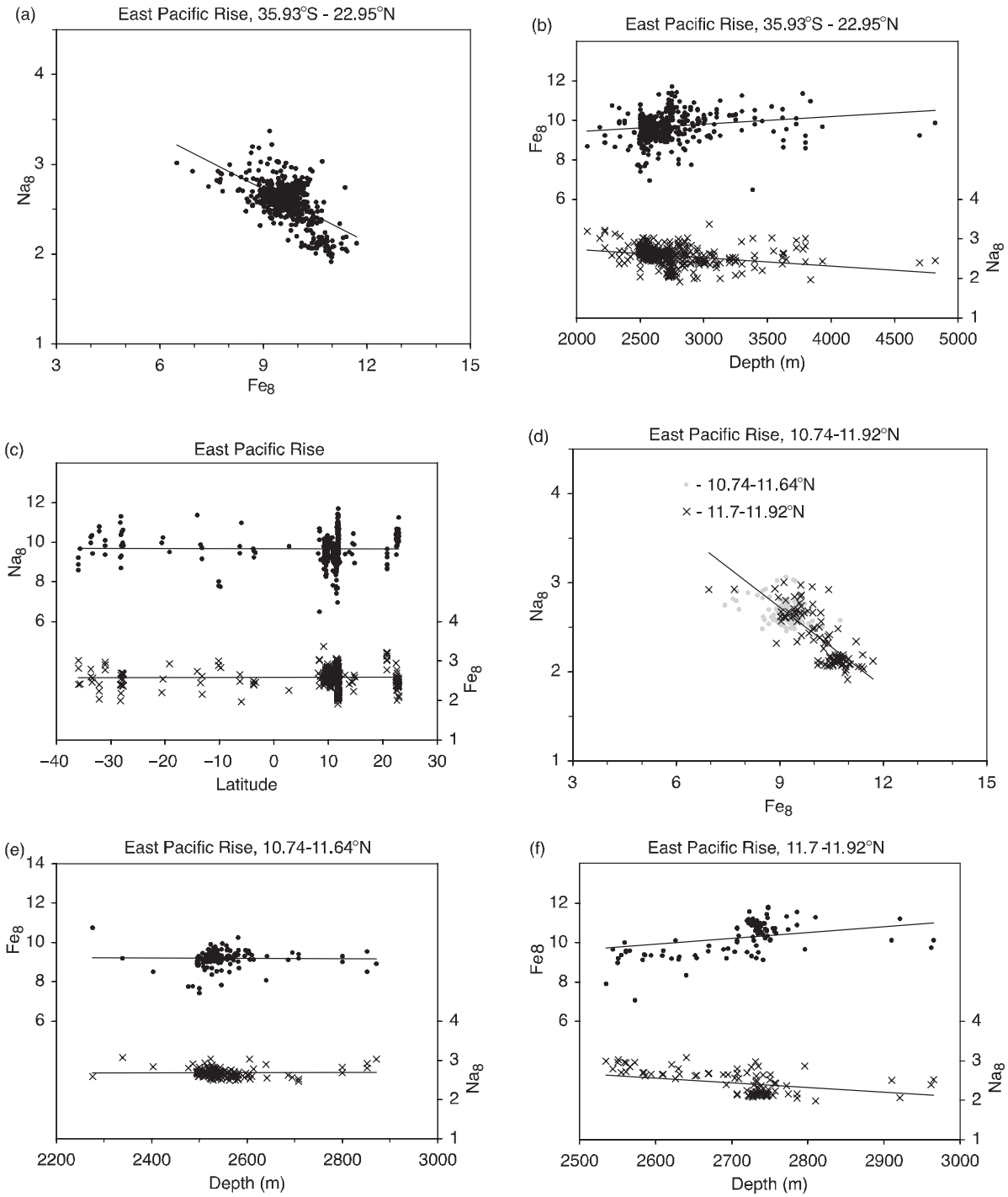

Fig. 7. East Pacific Rise. (a) Na_8 versus Fe_8 for 35·93°S to 22·95°N. (b) Na_8 and Fe_8 versus sampling depth for 39·53°S to 22·95°N. (c) Na_8 and Fe_8 versus latitude. (d) Na_8 versus Fe_8 for 10·74 to 11·92°N. The trend line is fitted to the data for 11·7 to 11·92°N. (e) Na_8 and Fe_8 versus sampling depth for 10·74 to 11·64°N. (f) Na_8 and Fe_8 versus sampling depth for 11·7 to 11·92°N.

systematic variation of either Na_8 or Fe_8 with depth (Fig. 7e). Immediately to the north at 11·7–11·92°N, a ridge segment only 24 km long, Na_8 and Fe_8 show a clear inverse relationship (Fig. 7d), an increase of Fe_8 with depth, and a decrease of Na_8 with depth (Fig. 7f). The obvious high quality of the depth correlations for this segment appears to be a result of precise depth information obtained by the *Alvin* submersible, and the variation of both Na_8 and Fe_8

with depth is the opposite of the Klein & Langmuir (1987, 1989) and Langmuir *et al.* (1992) modeling. However, the precise depth measurements may simply be the result of sampling a stratigraphic sequence of lavas exposed by a fault scarp, and therefore may have little relationship to axial depth. This possibility emphasizes the large uncertainties in the interpretation of samples from structurally complex ridges in which the spatial relationships of the lava flows cannot be mapped as they would be on land. In our modeling, the excellent inverse correlation of Na_8 vs Fe_8 (Fig. 7d and f) for a ridge segment only 24 km long indicates significant mantle heterogeneity at a very small scale. We have not found this feature in the Atlantic despite a search of short ridge segments with large amounts of data, some with similarly precise depth information obtained by the *Alvin* submersible.

Galapagos Ridge

The minimum depth along the east–west-trending Galapagos Ridge occurs at about 91·3–92°W (Detrick *et al.*, 2002). In the Smithsonian file, almost all the analyses of Galapagos Ridge basalts are concentrated at 93·6–96°W and 85·1–87·2°W (Fig. 8b), two restricted regions that lie on opposite sides of the minimum depth. The Smithsonian data show no significant variation of Na_8 and Fe_8 with depth (Fig. 8a), but the geographical distribution of the samples is poor for determining such trends. Therefore, we rely on the diagrams of Langmuir *et al.* (1992, fig. 19) and Detrick *et al.* (2002, fig. 3), both of which indicate that the chemistry vs depth systematics are the opposite of the Klein & Langmuir (1987, 1989) and Langmuir *et al.* (1992) modeling. For a very small segment of the ridge (about 50 km), the Smithsonian data show a clear inverse trend of Na_8 vs Fe_8 (Fig. 8c) similar to the inverse trend for a short segment of the East Pacific Rise (Fig. 7d). Furthermore, the spread of Na_8 and Fe_8 values covers most of the full global extent of the inverse Na_8–Fe_8 variation. This is inconsistent with the Klein & Langmuir (1987, 1989) and Langmuir *et al.* (1992) model because it implies the existence of most of the full range of their proposed oceanic potential temperatures within a ridge distance of only about 50 km. However, in our interpretation, it simply indicates strong short-range mantle heterogeneity at this locality.

Juan de Fuca and Gorda Ridges

The Na_8–Fe_8 plot for the combined Juan de Fuca and Gorda ridges (Fig. 9a) shows no clear trend, either positive or inverse. Even for samples from a very short ridge segment (Fig. 9b), the amount of scatter is essentially the same. These features indicate a mantle source that is heterogeneous at short distances, a result shared by the East Pacific Rise and Galapagos Ridge. The lack of any clear variation of Fe_8 and Na_8 with depth (Fig. 9c) is similar to plots for the South Atlantic data, and provides no support for the Klein & Langmuir (1987, 1989) and Langmuir *et al.* (1992) modeling. The only variation is a slight northward decrease of Fe_8, but there is no corresponding change in Na_8 (Fig. 9d).

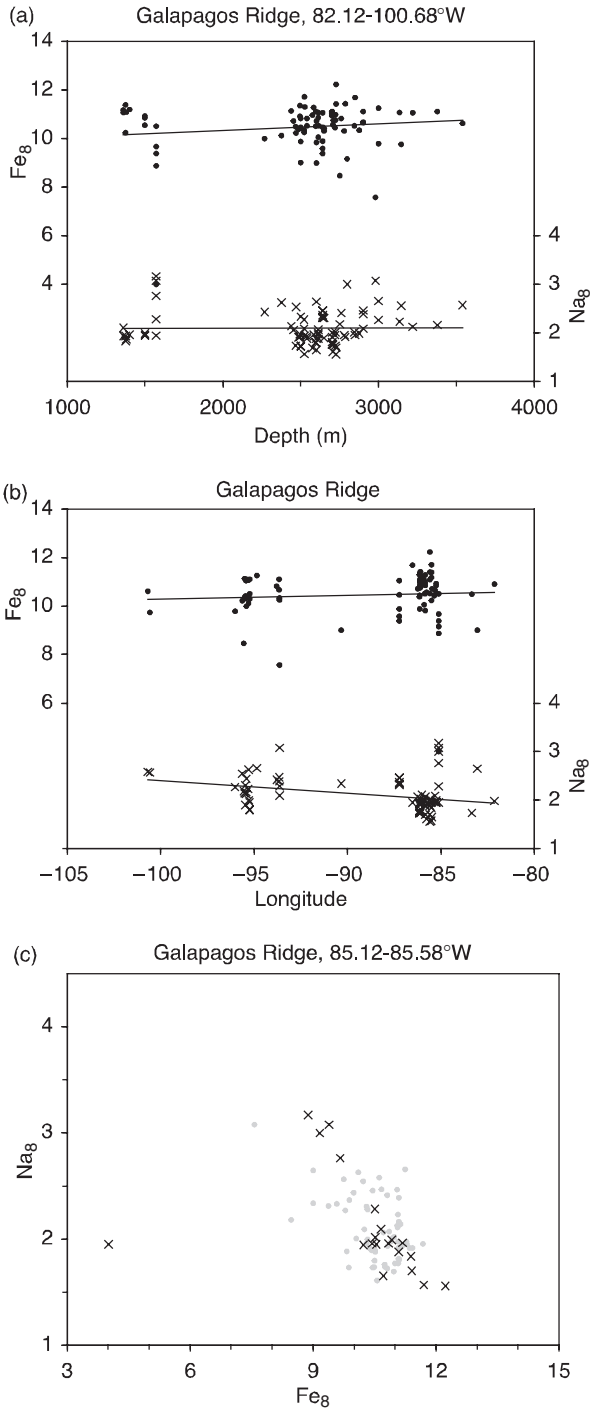

Fig. 8. Galapagos Ridge. (a) Na_8 and Fe_8 versus sampling depth; all data. (b) Na_8 and Fe_8 versus longitude; all data. (c) Na_8 versus Fe_8; crosses are samples from 85·12 to 85·58°W; gray circles are all other Galapagos samples.

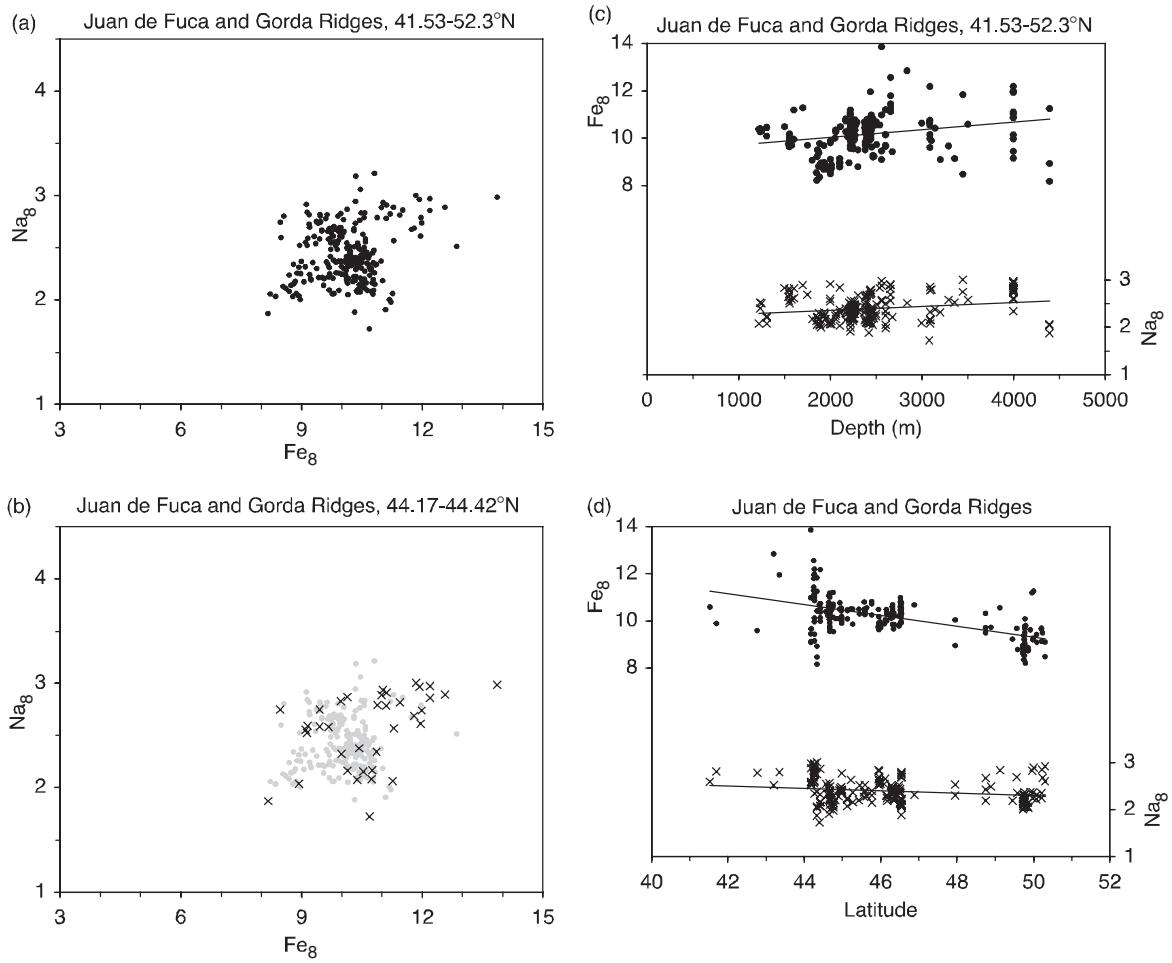

Fig. 9. Juan de Fuca and Gorda Ridges. (a) Na_8 versus Fe_8; all data. (b) Na_8 versus Fe_8; crosses are data from 44·17 to 44·42°N. Gray circles are all other Juan de Fuca and Gorda Ridge data. (c) Na_8 and Fe_8 versus axial depth. (d) Na_8 and Fe_8 versus latitude.

Carlsberg Ridge and Red Sea Rift

Data for Na_8 and Fe_8 for the Carlsberg Ridge and Red Sea Rift show two distinct clusters (Fig. 10a), neither of which shows any trend with depth (Fig. 10b). For the Carlsberg Ridge, there is also no significant variation of Na_8 or Fe_8 with latitude (Fig. 10c). The combined plot of Na_8 vs Fe_8 (Fig. 10a) for these two areas has the same form as the rough inverse correlations for the Atlantic (Fig. 2) and East Pacific Rise (Fig. 7a). We interpret the two distinct clusters as an indication of a difference in the composition of the mantle between the Red Sea and the northern Indian Ocean. The northern Indian Ocean is also fairly typical of oceanic areas generally (compare Figs 10b and 11a). Also, the higher Fe_8 (lower MgO/FeO) values for the Red Sea basalts are consistent with the occurrence of peridotite samples from off-craton localities that extend to lower Mg numbers than abyssal peridotites from the ocean basins (Walter, 2004). This general consistency between Fe_8 values for basalts and MgO/FeO ratios of peridotites from the same areas is a strong argument in support of mantle heterogeneity as the explanation for the Na_8–Fe_8 variations of MORBs.

Global

The global plot of Na_8 vs Fe_8 shows an overall inverse trend that is made more diffuse by the positive trends (Fig. 11a). The slight dominance of the inverse trend over the positive trends is driven by the extreme values for the Cayman and Reykjanes–Iceland–Kolbeinsey data. In terms of the model proposed here, this appears to indicate that mantle heterogeneity has a slightly stronger influence on MORB chemistry than progressive separation of melts from short rising diapirs.

As discussed above, the Smithsonian database shows no ridge of any length for which the correlations of both Na_8 and Fe_8 with depth are fully consistent with the Klein & Langmuir (1987, 1989) and Langmuir *et al.* (1992) modeling. However, when the global data are all plotted together

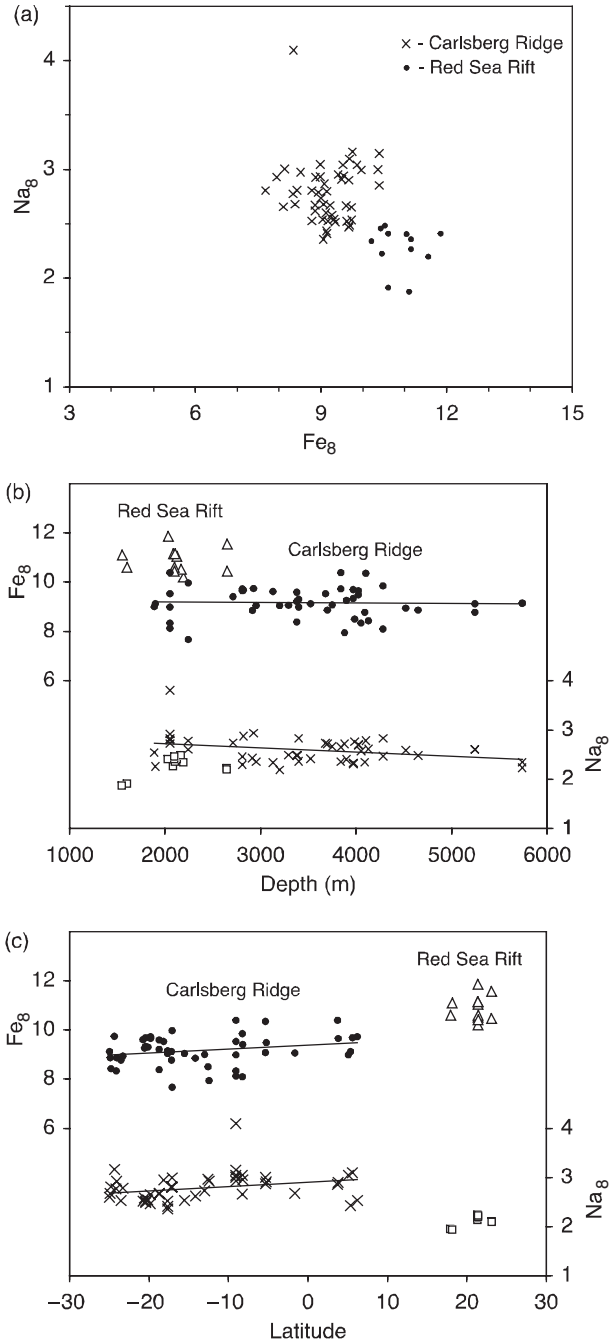

Fig. 10. Carlsberg Ridge and Red Sea Rift. (a) Na_8 versus Fe_8. (b) Na_8 and Fe_8 versus sampling depth. (c) Na_8 and Fe_8 versus latitude.

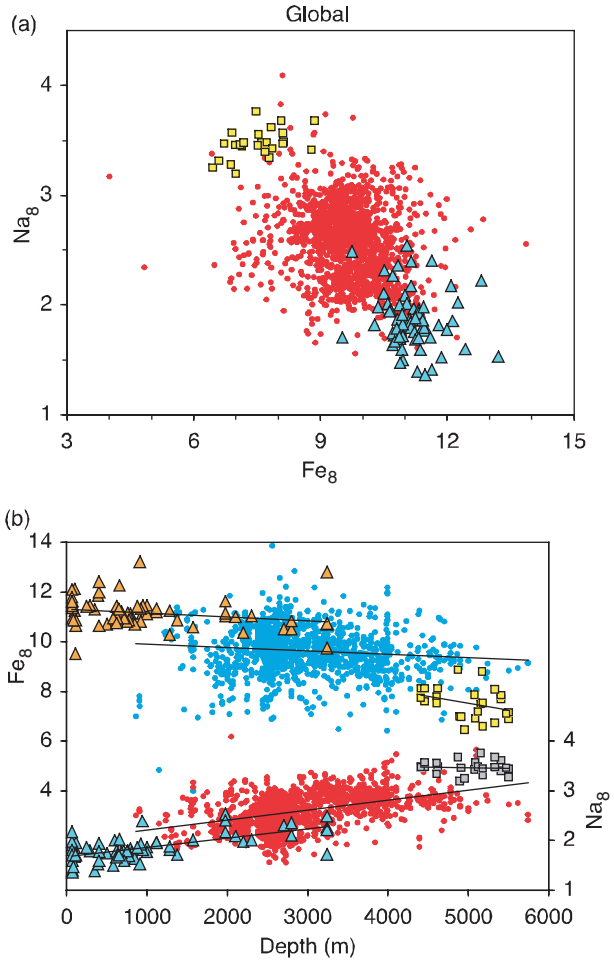

Fig. 11. Global data for all ridges. (a) Na_8 versus Fe_8. Yellow squares are data from the Mid-Cayman Rise. Blue triangles are data from the Reykjanes Ridge, Iceland, and the Kolbeinsey Ridge, repeated from Fig. 4c. Red circles are all other data. (b) Na_8 and Fe_8 versus sampling depth. Circles are data from Figs. 4a, 4b, 4d, 6b, 8b, 9b, 10c, and 11b. Triangles are data from the Reykjanes Ridge, Iceland, and the Kolbeinsey Ridge, repeated from Fig. 4c. Squares are data from the Mid-Cayman Rise.

(Fig. 11b), there appears to be a rough Na_8 increase and Fe_8 decrease with depth, as Klein & Langmuir (1987) originally showed. This seems to be an inconsistency. Data in the central part of the plot (blue and red dots) constitute almost all of the global data, the combined results of Figs 4a, 6b, 7b, 8a, 9c and 10b. These widely scattered data, taken together, show a weak increase of Na_8 with depth and a very weak or possibly nonexistent decrease of Fe_8 with depth, a result consistent with the plots of ridge segments of 'global' length that show no consistent depth correlation. The two extreme data sets, Cayman and Reykjanes–Iceland–Kolbeinsey, which drive the appearance of an overall global correlation of increasing Na_8 and decreasing Fe_8 with depth, are clearly offset from the crude trends of the main group of points in the central part of the diagram. These offsets are an expected result of source heterogeneity, but not of a smoothly continuous variation of potential temperature.

Given an adequate source of energy combined with an upper temperature limit, as proposed here, an enriched mantle source high in Fe would be capable of producing a greater volume of melt (thicker crust, which would contribute to a smaller axial depth) at relatively uniform

temperature than a source low in Fe (thinner crust, which would contribute to a greater axial depth). This is consistent with shallow to intermediate axial depths for the Reykjanes–Iceland–Kolbeinsey data and deep axial depths for the Cayman data. However, as axial depth is a complex function of both crustal and upper mantle density, the correlation of chemistry with depth is expected to be very rough and to contain reversals and offsets, as is observed.

PRESSURE–TEMPERATURE RANGE OF MELT EXTRACTION

We treat the extraction of MORB melts and their formation in the mantle as separate issues. The pressure range of extraction is indicated by the compositions of melts delivered to the surface. The maximum global range of Fe_8 values at a constant value of Na_8 is about 6·3 and occurs at a Na_8 value of about 2·5 (Fig. 11a, two outliers excluded). Figure 1 shows that if melts are generated in the pressure range of the plagioclase–spinel lherzolite solidus, this range of Fe_8 values permits a pressure range of only about ± 0·15 GPa. This corresponds to a very narrow temperature range of about ± 15°C. The reason for the narrow temperature range is the low dT/dP slope of the solidus in this pressure range.

Experimental studies of natural compositions have not reported the existence of the Na_8–Fe_8 systematics at the solidus of lherzolite, which confines the P–T range of observed magmas so tightly. There are two reasons for this. First, it is difficult even to approach the solidus in a study of a natural composition because the melt pockets become too small for analysis. Second, even if the solidus or near-solidus phase relations could be determined, the inverse Na_8–Fe_8 variation at nearly constant pressure would be detected only after a number of natural compositions were studied. In the absence of some hint that these relationships exist at the solidus in a narrow pressure range, it is understandable that a search to find them has never been mounted.

MAXIMUM PRESSURE OF MORB EXTRACTION

The projected six-space solidus surface in the CIPW normative basalt tetrahedron (Fig. 1) is the low-pressure boundary of a projected six-space solidus volume in the basalt tetrahedron that extends toward more olivine-rich compositions. This solidus volume for the spinel lherzolite assemblage, ol + opx + cpx + sp + liq, is limited at higher pressures by another bounding solidus surface that has the garnet–spinel lherzolite assemblage, ol + opx + cpx + sp + gt + liq. There would be projected isobaric surfaces at approximately constant MgO that would extend from the projected isobaric lines at 1·1 and 1·3 GPa shown in Fig. 1 into the interior of the spinel lherzolite projected solidus volume. Although these phase relations are not yet determined, their necessary general form indicates that the inverse and positive Na_8–Fe_8 variations would also occur at the solidus for pressures greater than those of the plagioclase–spinel lherzolite transition. The same kind of reasoning would apply at pressures below those of the plagioclase–spinel lherzolite transition. Thus, the solidus phase relations combined with the Na_8–Fe_8 systematics shown in Fig. 1 provide a tight limit only on the pressure range of melt extraction. They do not constrain the location of this pressure range.

The location of the pressure range requires a different approach. The CaO–MgO–Al_2O_3–SiO_2, CaO–MgO–Al_2O_3–SiO_2–Na_2O, and CaO–MgO–Al_2O_3–SiO_2–FeO versions of the tholeiitic basalt tetrahedron (Presnall *et al.*, 1979; Walter & Presnall, 1994; Gudfinnsson & Presnall, 2000) all show that as pressure increases, the higher pressure melts from spinel lherzolite and garnet lherzolite progressively migrate toward more magnesian and olivine-rich compositions as pressure increases. For these melts to reach the composition field of MORBs, crystallization of olivine at low pressures is required (see also Green & Falloon, 2005). However, no indication of a significant olivine-controlled crystallization path based on MORB glass analyses has ever been reported (Presnall, 1999, fig. 9; Presnall *et al.*, 2002, figs 6 and 7), a result that applies to glass analyses from Iceland, the Siquieros data of Perfit *et al.* (1996), and the Macquarie Island data of Kamenetsky *et al.* (2000). We exclude data from glass inclusions because of complications caused by post-entrapment diffusion (Gaetani & Watson, 2000). In contrast, glass compositions from the Puna Ridge of Kilauea Volcano in Hawaii show a clearly defined trend of low-pressure olivine-controlled crystallization (Clague *et al.*, 1995). For melts extracted from a lherzolite mineralogy, the only way to avoid olivine-controlled crystallization when these melts cool at low pressures is to extract them at pressures below those of the spinel lherzolite stability field. At these low pressures, melts crystallize olivine when they cool, but they also crystallize plagioclase ± spinel very soon after the appearance of olivine (Presnall *et al.*, 2002, and references therein). Thus, to avoid all but a very small amount of olivine-controlled crystallization at low pressures, melts must be extracted from their source at pressures less than ~1·5 GPa (Presnall *et al.*, 2002, figs 6, 9 and 12). This would correspond to temperatures of ~1250–1280°C.

As the Na_8–Fe_8 systematics require a narrow pressure range of MORB extraction, it follows that melts must be extracted at either uniformly high or uniformly low pressures. If the pressure range is uniformly high, then significant olivine-controlled crystallization would always occur when the melts ascend and cool at lower pressures.

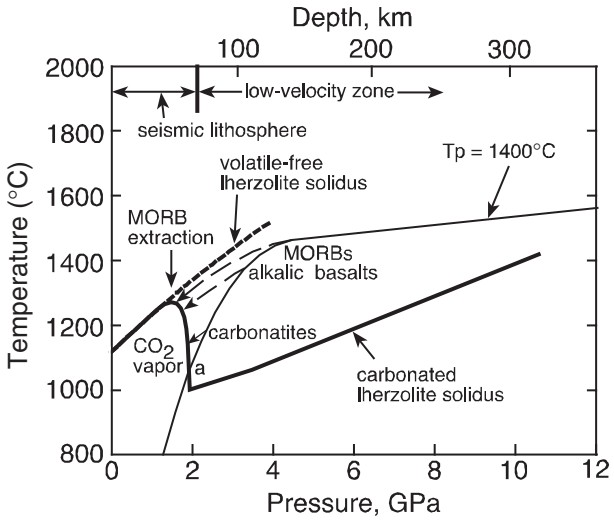

Fig. 12. Pressure-temperature diagram showing solidus curves for carbonated lherzolite and volatile-free lherzolite, after Fig. 1 of Presnall and Gudfinnsson (2005); based on the data of Hirschmann (2000), Dalton and Presnall (1998), Gudfinnsson and Presnall (2005) and Falloon and Green (1989).

This makes the absence of olivine-controlled fractionation trends at ridges (Presnall *et al.*, 2002, figs 6 and 12) an even stronger observation.

Melt extraction from a heterogeous mantle at uniform temperatures of ~1250–1280°C and pressures of ~1·2–1·5 GPa appears robust in its ability to explain the Na_8–Fe_8 systematics of MORBs on all parts of the oceanic ridge system, regardless of the proximity to presumed hot plumes such as Iceland, Azores, St. Helena, Tristan, Galapagos, Easter, and Afar. Because of the complete absence of any MORB glasses with a high-pressure, high-temperature compositional signature (high normative olivine) anywhere along the oceanic ridge system (Presnall *et al.*, 2002, figs 6 and 12), we conclude that these areas are not anomalously hot.

MORB FORMATION, RIDGE DEVELOPMENT, AND RIDGE DEATH

Melbourne & Helmberger (2002) found that the 405 and 660 km discontinuities between 40°N and 35°S beneath the East Pacific Rise show no observable temperature variation, and that no part of the ridge in this region could be supplied by material from the local lower mantle, even from a region as small as a single plume. This region includes the presumed Easter plume. As part of a detailed study of the upper mantle beneath the East Pacific Rise (MELT Seismic Team, 1998), Conder *et al.* (2002) found a distinctly asymmetrical distribution of S-wave velocities on the East Pacific Rise near 17°S, with velocities west of the ridge centered at ~70 km depth in the upper part of the low-velocity zone being lower than those east of the ridge. This asymmetry was explained by a melt source to the west of the ridge and eastward flow of this melt toward the ridge axis. Although the results from both of these studies appear to be robust, their application to ridges globally is untested. Nevertheless, these results and the many common features of all ridges suggest that ridge formation globally is an upper-mantle process confined roughly to the seismic lithosphere and the upper part of the low-velocity zone.

The normally assumed energy source for melting is adiabatic decompression. However, the unusually low dT/dP slope of the solidus in the plagioclase–spinel lherzolite transition (Presnall *et al.*, 2002, fig. 14) combined with the very narrow range of pressure indicated by the Na_8–Fe_8 systematics at the solidus would appear to allow an insufficient amount of decompression energy for magma generation in this pressure range. This apparent inconsistency assumes that if the compositions of melts produced at the surface indicate a fairly uniform T and P of separation from the source region, the amount of decompression that caused these melts in the mantle must be similarly small. We argue instead that magma formation is decoupled from magma extraction and that the pressure ranges for these processes are different. We propose a critical role for CO_2 and assume that the main effects of CO_2 are not significantly affected by small amounts of H_2O in the melts (Presnall & Gudfinnsson, 2005). Also, we assume that the oceanic lithosphere is subject to fractures that extend entirely through its thickness (Stuart *et al.*, 2007). Our petrological modeling that follows is inspired by and broadly consistent with the seismic modeling of Conder *et al.* (2002) and Dunn & Forsyth (2003).

The carbonated lherzolite solidus (Fig. 12) at pressures < ~1·8 GPa conforms closely to the volatile-free solidus. No crystalline carbonate phase is stable at these high temperatures. At about 1·8–1·9 GPa, the solidus of natural carbonated lherzolite abruptly drops in temperature by ~280°C (Falloon & Green, 1989) and then turns sharply back to a positive slope at greater pressures just as it meets the subsolidus stability curve for carbonate (not shown). Further discussion of these phase relations, first discovered by Wyllie & Huang (1975) and Eggler (1976), can be found in Eggler (1978) and Presnall & Gudfinnsson (2005). The steep portion of the solidus curve at ~1·8–1·9 GPa would shift a small amount in pressure depending on mantle composition but the solidus would retain its general form. The geotherm is for a mature oceanic area, which assumes a thermal boundary layer that extends to a depth of 140 km and a mantle adiabat with a potential temperature of 1400°C. The low-pressure part of the geotherm is consistent with heat flow model GDH2 of DeLaughter *et al.* (1999). The average depth to the base of the seismic

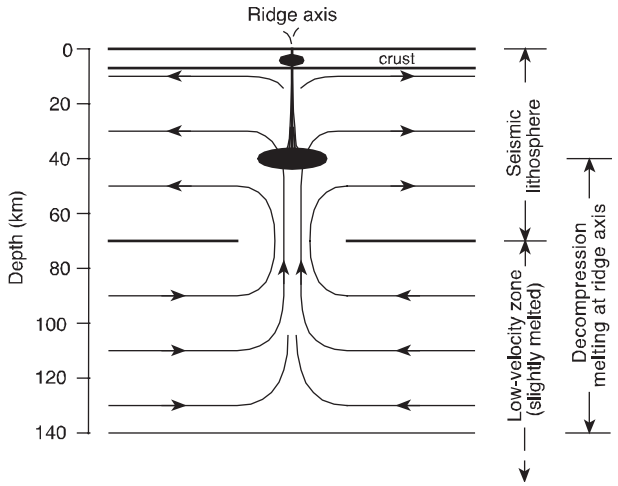

Fig. 13. Schematic diagram to illustrate lithosphere formation for the simplified case of a mid-ocean ridge that does not migrate. Varying rates of ridge migration would cause varying amounts of asymmetry, as modeled by Conder *et al.* (2002) for the East Pacific Rise. Arrows indicate directions of mantle flow. Black regions indicate melt extraction from the mantle, melt accumulation in a lower crustal magma chamber, and eruption of MORB magma and CO_2 vapor to the surface. The diagram does not address embedded mantle heterogeneities or the source of the asthenosphere.

lithosphere (G discontinuity) vs age in the Pacific Basin is fairly constant at about 68 km (Gaherty *et al.*, 1999), which is consistent with the thickness of young Pacific lithosphere determined by Weeraratne *et al.* (2007). This is the depth shown in Figs 12 and 13, and corresponds closely to the depth of the nearly vertical part of the solidus curve. Geotherms with steeper conductive gradients appropriate for younger lithosphere would intersect the solidus at nearly the same depth. This strongly suggests that the onset of low-temperature melting at essentially this depth for a mantle containing a small amount of carbonate is the cause of the G discontinuity.

We consider now the process of formation of a new ridge or extension of an existing ridge at a propagating rift tip such as the southward-propagating Eastern Volcanic Zone in southern Iceland. For a momentary opening of a fracture through the lithosphere at the leading tip of a propagating rift, the pressure drop at the intersection of the geotherm with the solidus curve would be about 1·9 GPa (Fig. 12, point a) just at the top of the partly melted low-velocity zone. Thus, venting of CO_2 to the surface would be explosive, even though the amount of CO_2 vented would be very small. Because of the nearly isobaric solidus slope at ~65 km, the escaping vapor produced by decompression across the solidus would initially have essentially the same temperature as its parent carbonate-rich melt in the low-velocity zone, but would cool along a vapor adiabat (not shown) on ascent to the surface. Although the proportion of carbonate-rich melt in the low-velocity zone would be very small, perhaps in the range of 0·05–0·2% (Presnall & Gudfinnsson, 2005, fig. 2), such melts are very fluid and would migrate at melt fractions as low as 0·05–0·1% (Minarik & Watson, 1995; Faul, 2001). However, for a momentary pressure difference of 1·9 GPa during the opening of a fracture and explosive flashing of CO_2-rich melt to yield CO_2 vapor, migration of fluids through a porous host-rock is almost certainly irrelevant. Instead, the rock would probably fracture with sudden escape of the liquid–vapor mixture. The CO_2-rich melts, as they exist in the mantle, would be carbonatitic (Gudfinnssoon & Presnall, 2005) but the detailed chemistry of the abrupt transformation to melt and vapor phases produced on sudden decompression is unknown. Even given this uncertainty, carbonate-rich deposits of some type would be expected at the surface. With successive explosive ventings of this type, the temperature where the geotherm crosses the nearly vertical solidus would eventually rise. Melts carried to the surface along with the CO_2 vapor would change (Fig. 12) to more voluminous alkalic basalts, and finally to tholeiitic MORBs (Gudfinnsson & Presnall, 2005). Because of the sharp bend of the solidus back to a positive dT/dP slope nearly coincident with the volatile-free solidus at about 1·2–1·7 GPa, the escape temperature of the vapor would not exceed ~1260–1280°C at ~1·4–1·5 GPa, which is within the estimated temperature–pressure range of the plagioclase–spinel lherzolite solidus for natural compositions. On the assumption of a solid adiabat gradient of 15°C/GPa, this is identical to our earlier potential temperature estimate of ~1240–1260°C (Presnall *et al.*, 2002) for MORB generation.

The expected sequence of magma types produced on progressive increase of temperature and maturity of a ridge is shown in part by the Eastern Volcanic Zone of Iceland (Saemundsson, 1979) and is consistent with experimental data (Gudfinnsson & Presnall, 2005). To the north where extension is occurring, the lavas are tholeiitic, but they become transitional to the south. Then, near the farthest visible limit of volcanism above sea level in the Westman Islands, the lavas become alkalic (Jakobsson, 1972). There is no indication of a further transition to carbonatites or carbonate-rich fluids, as expected from the experimental data of Gudfinnsson & Presnall (2005), but this would be likely to occur farther south on the ocean floor at the leading tip of the propagating ridge. Also, this would be expected at off-axis localities near mature spreading ridges where mantle temperatures are somewhat lower. Only one occurrence of venting of carbonate-rich fluids on the ocean floor is known (Kelley *et al.*, 2005), an off-axis locality near the Mid-Atlantic Ridge at about 30°N. The rarity of this occurrence may be due simply to the rarity of off-axis exploration with the *Alvin* submersible.

Along with periodic venting of CO_2 and a progressive rise in temperature, mass movement of the partly melted

rock in the low-velocity zone into the widening fracture would be expected, and melt compositions would change progressively from carbonate-rich to alkalic to tholeiitic. The steady-state condition of a mature spreading ridge would involve mass flow toward the ridge axis dominantly in the upper 70 km of the low-velocity zone, vertical ascent, melting, explosive escape of melt and CO_2 vapor at the ridge, and migration of the newly formed crust and depleted lithosphere away from the ridge axis (Fig. 13).

The new lithosphere, about 70 km in thickness, would require flow of a comparable amount of material from the upper part of the low-velocity zone into the region of melt formation directly beneath the ridge. Control by the phase relations on the maximum temperature for venting of CO_2 vapor would fix the steady-state temperature and pressure of magma extraction from the source at a relatively constant value of ~1·2–1·5 GPa, and eruption of melt and vapor would occur at the same time. Melt formation would extend to much higher pressures of ~4 GPa (Figs 12 and 13). Eruptions would occur only when driven by momentary opening of a fracture and explosive separation of CO_2 from the melt. This scenario is supported by the observation of H. J. B. Dick (personal communication, 2003) that vesicles are always present in MORB basalts at the scale of a single dredge haul. Also, Clague (2007) found that eruptions along the Juan de Fuca and Gorda Ridges show both strombolian and effusive deposits at every location examined. From fragments of curved glass films, he estimated the existence of gas bubbles up to 8 cm in diameter. In one locality, he found that a single explosive submarine eruption had distributed pyroclasts up to 3 km in all directions. This supports the view that explosive CO_2 escape is the vehicle that transports MORB melts to the surface. However, the abundant evidence for extensive low-pressure fractionation of MORB magmas (e.g. Walker *et al.*, 1979; Grove & Bryan, 1983; Grove *et al.*, 1992) indicates that vapor-assisted transport of melts from the source to the surface commonly does not occur as a single step.

Fracturing would gradually cease when lithospheric stresses shift to produce fracturing at a different locality. This would end the escape of CO_2, and the vehicle for bringing melt to the surface would disappear. The ridge would then die in favor of a new ridge at the new locality.

SUMMARY

The normalization procedure of Klein & Langmuir (1987) effectively removes the compositional variations of MORBs caused by low-pressure fractional crystallization. It yields Na_8–Fe_8 systematics in excellent agreement with the Na_2O–FeO systematics of solidus melts in the plagioclase–spinel lherzolite transition of the system CaO–MgO–Al_2O_3–SiO_2–Na_2O–FeO. An inverse correlation of Na_8 vs Fe_8 is interpreted as an indication of mantle source heterogeneity, whereas a positive correlation is explained by progressive extraction of melts from short, progressively depleted melting columns. These systematics indicate that the mantle source for mid-ocean ridges shows significant major-element heterogeneity over short distances in the eastern Pacific Ocean and over long distances in the Atlantic Ocean from 26°N to the Jan Mayen Fracture Zone. The Atlantic mantle from Bouvet to 26°N is fairly homogeneous. The Red Sea mantle is enriched in FeO/MgO relative to the northern Indian Ocean mantle.

A model is developed in which melting occurs over a large depth range extending into the upper part of the low-velocity zone, but melt extraction occurs only over a narrow pressure–temperature range centered at ~1·2–1·5 GPa and ~1250–1280°C. This narrow range is indicated by a combination of observed Na_8–Fe_8 systematics of MORBs and phase equilibrium constraints in the CaO–MgO–Al_2O_3–SiO_2–Na_2O–FeO system. The critical role of CO_2 vaporization and the unusual form of the lherzolite–CO_2 solidus curve in maintaining a uniformly low temperature and pressure of magma extraction for MORBs is supported by the recent observation (Clague *et al.*, 2003; Clague, 2007) that strombolian and effusive eruptions at ridges always occur together. These constraints on MORB generation are not consistent with the existence of hot plumes on or close to ridges. This includes Iceland, Azores, St. Helena, Tristan, Bouvet, Easter, Galapagos, and Afar.

Oceanic ridge formation is modeled as a process confined entirely to the seismic lithosphere and the low-velocity zone. In this modeling, ridge development starts by formation of a fracture through the oceanic lithosphere, which allows explosive venting of CO_2 vapor from the upper part of the low-velocity zone. This periodic venting progressively heats the lower lithosphere to produce initial carbonate-rich eruptions followed by alkalic basalts, and finally, for a mature and active ridge, tholeiitic MORBs. The slightly melted upper part of the seismic low-velocity zone flows toward the ridge, rises at the ridge axis, and melts further to produce MORB magmas. The depleted residue and new oceanic crust then migrate away from the ridge axis as new oceanic lithosphere. Ridges die in response to plate stresses that shift the formation of lithosphere fracturing to other locations. This shuts down the venting of CO_2 vapor and removes the vehicle for transporting melt to the surface.

ACKNOWLEDGEMENTS

Support was provided by National Science Foundation Grant EAR-0106645, the Geophysical Laboratory, and the Bayerisches Geoinstitut. We thank Henry Dick, Gillian Foulger, Shantanu Keshav, Tony Morse, Jim Natland, Mike Rhodes, and Mike Walter for very helpful comments on a preliminary version of the manuscript. D.C.P. thanks Don Anderson and Ian MacGregor for very stimulating

conversations on thermal issues and magma generation that provided the impetus for some of the modeling presented here. Paul Asimow provided a very useful formal review. We are especially pleased to be able to contribute to this volume in honor of the long and distinguished career of David Green.

REFERENCES

Batiza, R., Hékinian, R., Bideau, D. & Francheteau, J. (1995). Chemistry of deep (3500–5600 m) Pacific MORB—Why is the Pacific anomalous? *Geophysical Research Letters* **22**, 3067–3070.

Brodholdt, J. P. & Batiza, R. (1989). Global systematics of unaveraged mid-ocean ridge basalt compositions: Comments on 'Global correlations of ocean ridge basalt chemistry with axial depth and crustal thickness by E. M. Klein and C. H. Langmuir'. *Journal of Geophysical Research* **94**, 4231–4239.

Clague, D. A. (2007). Simultaneous effusive and strombolian eruptions along mid-ocean ridges. Geophysical Research Abstracts 9, abstract 02096.

Clague, D. A., Davis, A. S., & Dixon, J. E. (2003). Submarine strombolian eruptions along the Gorda mid-ocean ridge, In White, J. D. L., Smellie, J. L., & Clague, D. A. (eds) *Explosive Subaqueous Volcanism*, Monograph **140**, American Geophysical Union, pp. 111–128.

Clague, D. A., Moore, J. G., Dixon, J. E. & Friesen, W. B. (1995). Petrology of submarine lavas from Kilauea's Puna Ridge, Hawaii. *Journal of Petrology* **36**, 299–349.

Conder, J. A., Forsyth, D. W. & Parmentier, E. M. (2002). Asthenospheric flow and asymmetry of the East Pacific Rise, MELT area. *Journal of Geophysical Research* **107**, doi:10.1029/2001JB000807.

Dalton, J. A. & Presnall, D. C. (1998). Carbonatitic melts along the solidus of model lherzolite in the system $CaO–MgO–Al_2O_3–SiO_2–CO_2$ from 3 to 7 GPa. *Contributions to Mineralogy and Petrology* **131**, 123–135, doi:10.1007/S004100050383.

DeLaughter, J. E., Stein, S. & Stein, C. (1999). Extraction of the lithosphere aging signal from satellite geoid data. *Earth and Planetary Science Letters* **174**, 173–181, doi:10.1016/S0012-821X(99)00247-2.

Detrick, R. S., Sinton, J. M., Ito, G., Canales, J. P., Behn, M., Blacic, T., Cushman, B., Dixon, J. E., Graham, D. W. & Mahoney, J. J. (2002). Correlated geophysical, geochemical, and volcanological manifestations of plume–ridge interaction along the Galapagos spreading center. *Geochemistry, Geophysics, Geosystems* **3**, doi:10.1029/2002GC000350, 14 pp.

Dick, H. J. B., Fisher, R. L. & Bryan, W. B. (1984). Mineralogic variability of the uppermost mantle along mid-ocean ridges. *Earth and Planetary Science Letters* **69**, 88–106.

Dunn, R. A. & Forsyth, D. W. (2003). Imaging the transition between the region of mantle melt generation and the crustal magma chamber beneath the southern East Pacific Rise with short-period Love waves. *Journal of Geophysical Research* **108**, doi:10.1029/2002JB002217.

Eggler, D. H. (1976). Does CO_2 cause partial melting in the low-velocity layer of the mantle? *Geology* **4**, 69–72.

Eggler, D. H. (1978). The effect of CO_2 upon partial melting of peridotite in the system $Na_2O–CaO–Al_2O_3–MgO–SiO_2–CO_2$ to 35 kb, with an analysis of melting in a peridotite–$H_2O–CO_2$ system. *American Journal of Science* **278**, 305–343.

Falloon, T. & Green, D. H. (1989). The solidus of carbonated, fertile peridotite. *Earth and Planetary Science Letters* **94**, 364–370, doi:10.1016/0012-821×(89)90153-2.

Faul, U. H. (2001). Melt retention and segregation beneath mid-ocean ridges. *Nature* **410**, 920–923.

Foulger, G. R., Natland, J. H. & Anderson, D. L. (2005*a*). Genesis of the Iceland melt anomaly by plate tectonic processes. In: Foulger, G. R., Natland, J. H., Presnall, D. C. & Anderson, D. L. (eds) *Plates, Plumes, and Paradigms. Geological Society of America, Special Papers* **388**, 595–625.

Foulger, G. R., Natland, J. H., Presnall, D. C. & Anderson, D. L. (2005*b*). *Plates, Plumes, and Paradigms. Geological Society of America, Special Paper* **388**, 881 pp.

Gaetani, G. A. & Watson, E. B. (2000). Open system behavior of olivine-hosted melt inclusions. *Earth and Planetary Science Letters* **183**, 27–41.

Gaherty, J. B., Kato, M. & Jordan, T. H. (1999). Seismological structure of the upper mantle: a regional comparison of seismic layering. *Physics of the Earth and Planetary Interiors* **110**, 21–41.

Green, D. H. & Falloon, T. J. (2005). Primary magmas at mid-ocean ridges,'hotspots', and other intraplate settings: Constraints on mantle potential temperature. In: Foulger, G. L., Natland, J. H., Presnall, D. C. & Anderson, D. L. (eds) *Plates, Plumes, and Paradigms. Geological Society of America, Special Paper* **388**, 217–247.

Grove, T. L. & Bryan, W. B. (1983). Fractionation of pyroxene-phyric MORB at low pressure: An experimental study. *Contributions to Mineralogy and Petrology* **84**, 298–309.

Grove, T. L., Kinzler, R. J. & Bryan, W. B. (1992). Fractionation of mid-ocean ridge basalt (MORB). In: Phipps Morgan, J., Blackman, D. K. & Sinton, J. M. (eds) *Mantle Flow and Melt Generation at Mid-Ocean Ridges. Geophysical Monograph, American Geophysical Union* **71**, 281–310.

Gudfinnsson, G. H. & Presnall, D. C. (2000). Melting behavior of model lherzolite in the system $CaO–MgO–Al_2O_3–SiO_2–FeO$ at 0·7–2·8 GPa. *Journal of Petrology* **41**, 1241–1269.

Gudfinnsson, G. H. & Presnall, D. C. (2005). Continuous gradations among primary carbonatitic, kimberlitic, melilititic, basaltic, picritic, and komatiitic melts in equilibrium with garnet lherzolite at 3–8 GPa. *Journal of Petrology*, doi:10.1039/petrology/egi029.

Hirschmann, M. M. (2000). Mantle solidus: Experimental constraints and the effects of peridotite composition. *Geochemistry, Geophysics, Geosystems* **1**, doi:10.1029/2000GC000070.

Jakobsson, S. P. (1972). Chemistry and distribution pattern of Recent basaltic rocks in Iceland. *Lithos* **5**, 365–386.

Kamenetsky, V. S., Everard, J. L., Crawford, A. J., Varne, R., Eggins, S. M. & Lanyon, R. (2000). Enriched end-member of primitive MORB melts: Petrology and geochemistry of glasses from Macquarie Island (SW Pacific). *Journal of Petrology* **41**, 411–430.

Kelley, D. S., Karson, J. A., Früh-Green, G. L., Yoerger, D. R., Shank, T. M., Butterfield, D. A., Hayes, J. M., Schrenk, M. O., Olson, E. J., Proskurowski, G., Jakuba, M., Bradley, A., Larson, B., Ludwig, K., Glickson, D., Buckman, K., Bradley, A. S., Brazelton, W. J., Roe, K., Elend, M. J., Delacour, A., Bernasconi, S. M., Lilley, M. D., Baross, J. A., Summons., R. E. & Sylva, S. P. (2005). A serpentinite-hosted ecosystem: The Lost City hydrothermal field. *Science* **307**, 1428–1434.

Klein, E. M. & Langmuir, C. H. (1987). Global correlations of ocean ridge basalt chemistry with axial depth and crustal thickness. *Journal of Geophysical Research* **92**, 8089–8115.

Klein, E. M. & Langmuir, C. H. (1989). Local versus global variations in ocean ridge basalt composition: A reply. *Journal of Geophysical Research* **94**, 4241–4252.

Langmuir, C. H., Klein, E. M. & Plank, T. (1992). Petrological systematics of mid-ocean ridge basalts: Constraints on melt generation beneath ocean ridges. In: Phipps Morgan, J., Blackman, D. K. & Sinton, J. M. (eds) *Mantle Flow and Melt Generation*

at Mid-Ocean Ridges. Geophysical Monograph. American Geophysical Union **71**, 183–280.

Libourel, G. (1991). Chromium in basalts: An experimental study. *EOS Transactions, American Geophysical Union, Fall Annual Meeting* 547.

Liu, T.-C. & Presnall, D. C. (2000). Liquidus phase relations in the system CaO–MgO–Al_2O_3–SiO_2 at 2·0 GPa: Applications to basalt fractionation, eclogite, and igneous sapphirine. *Journal of Petrology* **41**, 3–20.

Mayzen, C. M., Toplis, M. J., Humler, E., Ludden, J. N. & Mével, C. (2003). A discontinuity in mantle composition beneath the Southwest Indian Ridge. *Nature* **421**, 731–733.

Melbourne, T. I. & Helmberger, D. V. (2002). Whole mantle shear structure beneath the East Pacific Rise. *Journal of Geophysical Research* **107**, 2204, doi:10.1029/2001JB000332.

MELT Sesimic Team, Imaging deep seismic structure beneath the mid-ocean ridge: The MELT experiment. *Science* **280**, 1215–1218.

Minarik, W. G. & Watson, E. B. (1995). Interconnectivity of carbonate melt at low melt fraction. *Earth and Planetary Science Letters* **133**, 423–437.

Niu, Y. & Batiza, R. (1991). An empirical method for calculating melt compositions produced beneath mid-ocean ridges: Application for axis and off-axis (seamounts) melting. *Journal of Geophysical Research* **96**, 21753–21777.

Niu, Y. & Batiza, R. (1993). Chemical variation trends at fast and slow spreading mid-ocean ridges. *Journal of Geophysical Research* **98**, 7887–7902.

Perfit, M. R., Fornari, D. J., Ridley, W. I., Kirk, P. D., Casey, J., Kastens, K. A., Reynolds, J. R., Edwards, M., Desonie, D., Schuster, R. & Paradis, S. (1996). Recent volcanism in the Siqueiros transform fault: picritic basalts and implications for MORB magma genesis. *Earth and Planetary Science Letters* **141**, 91–108.

Pertermann, M. & Hirschmann, M. M. (2003*a*). Partial melting experiments on a MORB-like pyroxenite between 2 and 3 GPa: Constraints on the presence of pyroxenite in basalt source regions from solidus location and melting rate. *Journal of Geophysical Research* **108**, doi:10.1029/2000JB000118, 17 pp.

Pertermann, M. & Hirschmann, M. M. (2003*b*). Anhydrous partial melting experiments on MORB-like eclogite: Phase relations, phase compositions and mineral–melt partitioning of major elements at 2–3 GPa. *Journal of Petrology* **44**, 2173–2201, doi:10.1039/petrology/egg074.

Presnall, D. C. (1969). The geometrical analysis of partial fusion. *American Journal of Science* **267**, 1178–1194.

Presnall, D. C. (1999). Effect of pressure on the fractional crystallization of basaltic magma. In: Fei, Y., Bertka, C. M. & Mysen, B. O. (eds) *Mantle Petrology: Field Observations and High Pressure Experimentation: A Tribute to Francis R. (Joe) Boyd. Geochemical Society, Special Publications* **6**, 209–224.

Presnall, D. C. & Gudfinnsson, G. H. (2005). Carbonate-rich melts in the oceanic low-velocity zone and deep mantle. In: Foulger, G. L., Natland, J. H., Presnall, D. C. & Anderson, D. L. (eds) *Plates, Plumes, and Paradigms. Geological Society of America, Special Paper* **388**, 207–216.

Presnall, D. C. & Helsley, C. E. (1982). Diapirism of depleted peridotite—a model for the origin of hot spots. *Physics of the Earth and Planetary Interiors* **29**, 148–160.

Presnall, D. C., Dixon, J. R., O'Donnell, T. H. & Dixon, S. A. (1979). Generation of mid-ocean ridge tholeiites. *Journal of Petrology* **20**, 3–35.

Presnall, D. C., Gudfinnsson, G. H. & Walter, M. J. (2002). Generation of mid-ocean ridge basalts at pressures from 1 to 7 GPa. *Geochimica et Cosmochimica Acta* **66**, 2073–2090.

Ritsema, J. & Allen, R. M. (2003). The elusive mantle plume. *Earth and Planetary Science Letters* **207**, 1–12.

Saemundsson, K. (1979). Outline of the geology of Iceland. *Jökull* **29**, 7–28.

Stuart, W. D., Foulger, G. R. & Barall, M. (2007). Propagation of the Hawaiian–Emperor volcano chain by Pacific plate cooling stress, In: Foulger, G. L. & Jurdy, D. M. (eds) *Plates, Plumes and Planetary Processes. Geological Society of America, Special Paper* 430 (in press).

Walker, D., Shibata, T. & DeLong, E. (1979). Abyssal tholeiites from the Oceanographer Fracture Zone. *Contributions to Mineralogy and Petrology* **70**, 111–125.

Walter, M. J. (2004). Melt extraction and compositional variability in mantle lithosphere. In: Holland, H. D., Turekian, K. K. (exec. eds) & Carlson, R. W. (vol. ed.) Treatise on Geochemistry, The Mantle and Core, 2. Amsterdam: Elsevier, pp. 363–394.

Walter, M. J. & Presnall, D. C. (1994). Melting behavior of simplified lherzolite in the system CaO–MgO–Al_2O_3–SiO_2–Na_2O from 7 to 35 kbar. *Journal of Petrology* **35**, 329–359.

Weeraratne, D. S., Forsyth, D. W., Yang, Y. & Webb, S. C. (2007). Rayleigh wave tomography beneath intraplate volcanic ridges in the South Pacific. *Journal of Geophysical Research* **112**, B06303, doi:10.1029/2006JB004403.

Wyllie, P. J. & Huang, W. L. (1975). Influence of mantle CO_2 in the generation of carbonatites and kimberlites. *Nature* **257**, 297–299.